Egypt.J.Chem. **Vol. 62**, No. 12. pp. 2313 - 2329 (2019)

Egyptian Journal of Chemistry
http://ejchem.journals.ekb.eg/

Low-cost Bio-Adsorbent Based on Amorphous Carbon Thin Film/ Chitosan Composite for Removal of Methylene Blue Dye from Aqueous Solutions: Kinetic and Isotherm

Mohamed Keshawy*[1], Mahmoud F. Mubarak[1], Amany Gaffer[1], R. Hosny[2], Th. Abdel Moghny[1]

[1]*Petroleum Applications Department, Egyptian Petroleum Research Institute (EPRI), 1 Ahmed El-Zomer, Nasr City, Box.No. 11727, Cairo, Egypt.*

[2]*Production Department, Egyptian Petroleum Research Institute (EPRI), 1 Ahmed El-Zomer, Nasr City, Box.No. 11727, Cairo, Egypt.*

IN this article, we focused on using low-cost bio-adsorbents such as chitosan from shrimp & crabs shells waste, and amorphous carbon thin film ACTF from microcrystalline cellulose waste, to prepare a new composite (ACTF/C) for removal of methylene blue (MB) dye from aqueous solution. ACTF/C composite was prepared via a novel ultrasonic co-precipitation method instead of traditional chemical vapor deposition (CVD) method. The morphological and structural descriptions are performed using XRD, FTIR, TEM, TGA, SAED and SEM analysis. The analysis results showed that the ACTF/C composite was prepared successfully. The effects of several parameters such as adsorbent doses (0.05–0.2 g/100 ml), temperatures (25–45 °C), initial solution pH of solution (3–9) , dye concentrations (10,25, 50, and 100 ppm) and contact time (20-80 min) on the adsorption process were examined. The kinetics, thermodynamic analyses, and adsorption isotherm models were examined to estimates the empirical results. The empirical facts are properly equipped with the Langmuir isotherm (R^2 = 0.997), giving an absorption capacity of more than 85mg/g. From kinetic details, we found that adsorption of methylene blue day across ACTF/C composite is represented by the pseudo-second-order model. In general, these outcomes suggest that the new ACTF/C composite provides great potential to get rid of methylene blue dye from contaminated water.

Keywords: ACTF/Chitosan composite, Ultrasonic Co Precipitation, Adsorption, Methylene blue dye, Kinetic.

Introduction

Water contamination is a noteworthy worldwide issue which requires progressing assessment and modification of water asset strategy at all levels. Environmental pollution caused by industrial effluents such as dyes has a great concern in the last decades[1]. Dyes are one of the most significant and serious sources of ecological pollution[2]. Toxic dyes are kept for a long time in water bodies; thus, these dyes can cause cancer, dermatological diseases and eventually affect human health[3, 4].

Many of the Delta governorates in Egypt are famous for electricity generation, spinning and weaving industries, and fruit packing. There are also, many other industrial activities such as the production of paint materials, silk fibers, and chemicals. In addition, agriculture is considered the main activity of the citizens surrounding the industrial zone. Egypt Spinning & Weaving is one of the largest companies in the middle of Delta in Egypt[5]. Therefore, the importance of this research is to study the effect of wastewater from textile factories and various chemical factories on the health of citizens and on the production of important agricultural crops in the Delta region

*Corresponding author e-mail: elkeshawy2006@yahoo.com; Telephone No:+2 01003722660
Received 13/3/2019; Accepted 29/5/2019
DOI: 10.21608/ejchem.2019.10428.1685

of Egypt[6, 7]. For these reasons, and due to the increase in industrial activities, drinking water stations in the Nile Delta governorates should be continuously purified due to the high prevalence of parasites in this area to ensure the safety of citizens. Accordingly, we used methylene blue dye, as an example of toxic waste discharged into Nile waters.

Methylene blue represents a raw material used in many industries such as paper, plastic, paint, leather, and textiles[8]. Methylene blue can also be produced as a polluted substance or as toxic waste discharged out from untreated effluents of these industries[9].

Methylene blue also has a toxic and carcinogenesis effect on human health and living organisms[10]. To a certain extent, MB enters our bodies through food, drinking water, air and can lead to poisoning at higher concentrations. Poisoning of methylene blue could have resulted from drinking-water contamination, high ambient air concentrations near emission sources, or intake via the food chain.

The elimination of methylene blue dye is extremely important for human life and the preservation of the environment. Varied chemical and physical methods such as; adsorption, coagulation, precipitation, and oxidation were advanced for the elimination of dyes from contaminated water Adsorption process is one of the most efficient methods for the removal of dyes from contaminated water. Due to its low cost, simplicity of design, easiness of procedure and insensitive to venomous substances.

Chitosan, is a biopolymer including NH_2 and OH functional groups as shown in Fig. 2, has been applied as a sorbent to eliminate heavy metals[11, 12], proteins[3, 13], and dye[14]. Utilization of chitosan as an adsorbent is restricted by its low surface area, colloid formation water, dissolution in acidic solutions, and degradation by chemical agents and action of microbes[14, 15]. Activated carbon (AC) is one of the best and most efficient approaches to wastewater remediation [16]. Its advantage with big surface area, high pore value, and convenient pore distribution, high surface reactivity which was produced as a result of the carbonization procedures and used on the high carbon content. Accordingly, we will develop the bio-composites in the form of chitosan with absorbent materials as activated carbon (AC) to minimize the total cost of the adsorbent, in addition to the possibility of exploiting agricultural residues in the production of activated carbon[17, 18].

The growing trend, is the main objective of this research via modification of rice straw lignocellulosic agriculture waste to prepare the activated carbon thin film (ACTF), then combine it with chitosan to attain on multifunctional activated carbon/chitosan (ACTF/C) composite, using Ultrasonic co-precipitation method instead of traditional chemical vapour deposition (CVD) method. After that, the equilibrium sorption data of the appropriate composite were evaluated to remove MB dye as toxic waste discharged into Nile waters, using commonly Langmuir and Freundlich adsorption isotherms models.

Experimental and Methods

Materials

The materials were used in this work were shrimp and crab shells,rice straw, sodium hydroxide (>99%purity), acetic acid (>99% purity), all other chemicals such as, CaMgO, sulfuric acid, acetone, hydrochloric acid-methanol, and sodium hypochlorite were supplied from Sigma–Aldrich and used as received. Methylene blue (MB) was obtained from Sigma–Aldrich, the molecular weight is M.wt319.85 g/mol, the chemical formula is ($C1_6H_{18}Cl\ N_3S$), and its chemical structure is shown in Fig. 1.

Catalyst preparation

Co silicate catalysts were prepared by addition of 1 wt% Co: Silicate, the produced supported silica was crushed, sieved up to 10–30 nm, and calcined at 700 °C for 3 h prior to impregnate. After that, the Co salt impregnated onto the supportd silica in 200ml ethanol, followed by calcinations under flow air (ca. 150 ml/min) at 650 °C for 7 h. The obtained solid was washed with distilled water and dried at 110 °C in air overnight [19, 20].

Preparation of the activated carbon thin film "ACTF" adsorbent from cellulose

At first, rice straw as cellulose source was de-lignified using a mixture of acetone and methanol 20 %. Secondly, basic hydrolysis of cellulose by traditional methods using (15% wt/v NaOH) to produce de-lignified microcrystalline cellulose. After that, 2g of the obtained microcrystalline cellulose (80% crystallinity) was carbonized by

(0.01 g CaMgO in 150 ml methanol at 40 °C for 2h, then it was left to evaporate at 80°Cfor 3h at least. Finally, the cellulose crystals mixture sprayed with conc. H_2SO_4 at a flow rate of 5 ml/min for 6 min. The resulted ACTF was filtered and washed with500 ml distilled water till pH becomes neutral and dried for 24 h[7, 21].

Preparation of chitosan

Chitosan was prepared from chitin. The chitin extraction process from crab and shrimp shells involves purification, demineralization, and de-acetylation.In the purification process at first, we remove any foreign materials by washing the crab and shrimp shells, after that the material was blended with a solution of sodium hypochlorite (NaOCl) (0.36% v/v) under stirring to remove any pigments. In the end, the materials were dried out in an oven for about 24 h up to70°C followed by mashing in a sieve to get particle sizes in the range order between about 0.297-0.5 mm. The obtained sample was demineralized using a mixture of(5% sodium hypochlorite and 7% hydrochloric acid). After that, they were soaked for 24 h to remove minerals. The above samples were treated with 100 ml of 10% sodium hydroxide for 4h. The De-acetylation process was carried out by adding 50% sodium hydroxide to the obtained sample and refluxing for 3 h at 120°C, then they were washed with 50% sodium hydroxide and filtered to obtain chitosan[22].

Ultrasonic Co-precipitation of ACTF/C Composite

Briefly, 5 g of chitosan was dissolved in 100ml of acetic acid solution (2% v/v) in an ultrasonic bath for 20 min at room temperature. Another solution of ACTF (0.1g +100 ml distilled water) was sonicated for 10 min at sonication power 100 watts and a frequency of 24 HZ in a water bath at room temp. The two solutions were then mixed together and stirred for 30 min then, the temperature raised up to 40 °C for 20 min, as shown in Fig. 3. The prepared composites were allowed to cool and recrystalized overnight, then filtered and dried for 3 h at 80-90°C.

Characterization

Fourier transform infrared spectroscopy

The Fourier transform infrared spectroscopy (FTIR) spectra of pure ACTF, chitosan and ACTF/C was carried out by using FTIR spectrophotometer (Nicolet IS-10 FTIR) between 600 and 4000 cm^{-1}.

X-ray diffraction studies

The measurements of X-ray diffraction (XRD) for the preparation materials have been carried out using advance diffractometer (PAN analytical XPERT-PRO) equipped with Cu-K radiation source (X = 0.154 nm). The diffraction data were collected in the range of 2= 2–60°using fixed time mode with a step interval of 0.05°

Transmission electron microscopy (TEM)

Nano-composites have been performed by using TEM (JEOL-JSM, 2100, Japan).TEM samples were prepared and placed in a sonicator to disperse the composite powders in methanol. A drop of the suspended sample was put on a TEM support grid (300 mesh copper grid coated with carbon). After drying in the air, the composite powder kept attached to the grid and was examined under the transmission electron microscope.

Scanning electron microscope (SEM)

The surface morphology of the chitosan and ACTF/C composite were examined using a scanning electron microscope (SEM) (Jeol, Model JSM5300).

Thermogravimetric analysis (TGA)

TGA of ACTF, chitosan and ACTF/C were carried out by using Q 600 SDT simultaneous DSC-TGA in a nitrogen atmosphere. The heating rate was 10°C/min with a heating range of 30–830°C.

Adsorption experiments

A stock MB dye solution of 1000 ppm was carried out by dissolving (1g) of MB dye in a liter of deionized water. Then the stock MB dye solution (as toxic waste waters) was distributed individually in 100cm^3 volumetric conical flasks. The pH of the MB dye solution was adjusted by the addition of HCl and 0.1 M NaOH solution.100 ml solution was used in every experiment for the removal of the dye from the water solutions. Then different ACTF/C composite doses (0.05-0.2 g/100 ml) were added up to each flask then stirred up to120 rpm, until reach dynamic equilibrium. The UV-Vis Spectrophotometer was utilized to determine the concentrations of MB dye in solution. The concentration of the MB dye in liquid before and after adsorption was measured via UV-visible spectrometer at 665 nm by extracting samples at a fixed interval time, as shown in Fig. 4. The amount of MB adsorbed per unit weight of adsorbent, q_t (mg/g), was calculated

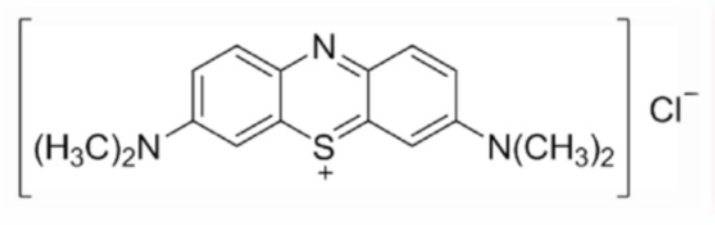

Fig. 1. Chemical structure of Methylene Blue.

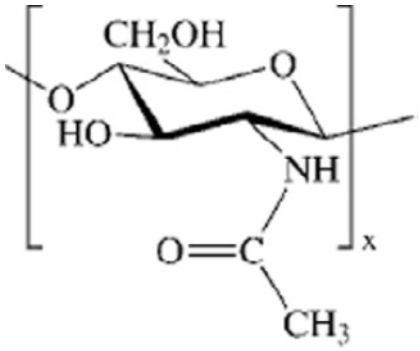

Fig. 2. Chemical structure of chitosan.

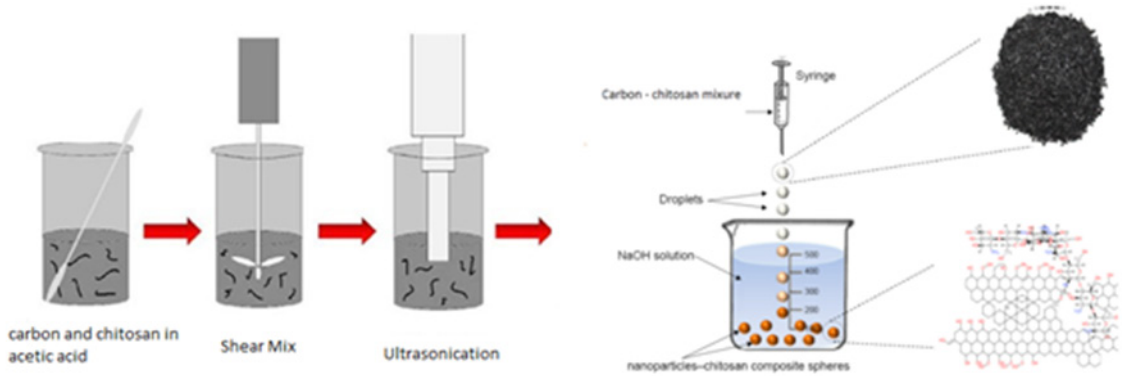

Fig. 3. Scheme of Ultrasonic co precipitation of ACTF/C composite preparation.

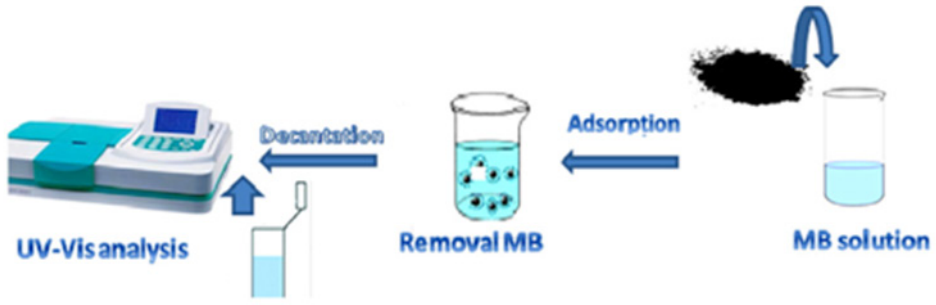

Fig. 4. Adsorption scheme of MB on ACTF-C composite.

using the following equations:

$$q_t = (C_0 - C_t)V/m \quad (1)$$

$$Adsorption\ (\%) = (C_0 - C_t)/C_0 \times 100 \quad (2)$$

where, C_o: initial concentration of MB dye; C_t: residual concentration of the MB dye after adsorption, V: volume of solution (ml), m: the amount of sorbent (ACTF/C composite)used in adsorption(g).

Adsorption isotherm

The relations between the adsorption of MB dyes on ACTF/C composite adsorbent surface were explained using Freundlich and Langmuir adsorption isotherm models.

Langmuir isotherm

Langmuir isotherm describes quantitatively the formation of a monolayer adsorbate on the outer surface of the adsorbent, and after that no further adsorption takes place. Thereby, the Langmuir represents the equilibrium distribution of MB between the ACTF/C composite and contaminated water. The monolayer adsorption is approved by Langmuir isotherm especially onto a surface containing a limited number of identical sites. Such a model assumes similar energies of adsorption onto the surface and no migration of the adsorbate in the plane of the surface. Based upon these assumptions, Langmuir can be written as the following equation[23]:

$$\frac{1}{q_e} = \frac{1}{q_m} + \frac{1}{K_L q_m C_e} \quad (3)$$

where K_L is the Langmuir isotherm constant (L/mg), q_e is the concentration of MB adsorbed at equilibrium (mg/g). C_e is the concentration of MB in the solution at equilibrium (ppm), C_o is the initial concentration of MB (ppm), q_m is maximum load covered the monolayer (mg/g).

The form of this isotherm can also be explained in terms of separation factor (R_L), as follows [23]:

$$R_L = \frac{1}{1+K_L C_0} \quad (4),$$

Freundlich isotherm

The Freundlich equation for a heterogeneous surface system is provided by Eq. (5)

$$\ln q_e = \ln K_F + \frac{1}{n} \ln C_e \quad (5),$$

where, K_F is Freundlich constants indicating capacity and n is the Freundlich constant indicating adsorption intensity, determined from the plot of $\ln q_e$ versus $\ln C_e$. The variables K_F and 1/n are related to sorption capacity and the sorption intensity of the system. The value of the term (1/n) offers a sign of the favorability of the sorbent-adsorbate system[24].

Desorption and regeneration studies

2 g of contaminated composites scattered in 100 ml of distilled water and 1% HCl at a temperature and speed of approximately 25 ° C and 150 rpm. The prepared solution leaves 120 minutes to a balance and reaches a maximum desorption rate. Then 1 ml sample is taken every 10 minutes to determine the rest of the day or by-products removed in distilled water and HCl using a UV device. The above procedure is repeated for 6 cycles to study the regeneration of prepared adsorbent (ACTF/C) composite[25].

Results and Discussion

Characterization of ACTF/C composite

FTIR Analysis

FTIR spectra of Nanocrystalline, amorphous carbon film thin spectrum (ACTF) was represented in Fig. 5 (a), where the band at 3431 cm^{-1}& 1100 cm^{-1}indicate the presence of functional group OH, and stretch C = O. The characteristic bands at 671, 802 cm^{-1}clarifythe aromatic mono-substituted and aromatic ring of the amorphous carbon film. Moreover, the peak at 1627 cm^{-1} is corresponding to the oxidation of ACTF[26].

FTIR of chitosan in Fig. 5(b), showed hydroxyl (OH) peaks at 3306.35 cm^{-1}, intensive peaks detected around 1628.87 cm^{-1}, 1540.02 cm^{-1} and 1419.16 cm^{-1}exposing the existence of(C = O amide bond), N-H bending and C-H distortion correspondingly[27].

FTIR spectra of ACTF/C in Fig. 5(c), exhibited, at 1492 cm^{-1}, 843 cm^{-1} and 755 cm^{-1}, this may due to present of carbonate vibration modes. Complementary bands of water adsorbed were also noticed at 3446 & 1637 cm^{-1}. The existence of organic substance can be assumed from the look of a band in the region of 2924-2867 cm^{-1}. In the spectrum of ACTF/C compounds, the characteristic bands at 1675 cm-^{1} (C = O of the amide bond) between ACTF and chitosan. The peak appears at 1068 cm^{-1}, may attribute to the symmetrical elongation of CO_3^{-}. Two other bands refer to association bands, that is, ν 1 + ν 4 at 1870 cm $^{-1}$ and 2850 cm $^{-1}$.

XRD Analysis

The amorphous nature of the ACTF was determined using the intensity of the observed rays with respect to the scattering angle (2θ). XRD pattern of ACTF in Fig. 6(a), displayed broad asymmetric peaks corresponding to 2θ = 23.5°andassigned as the C(002) which express the existence of the hexagonal graphite configuration[17]. In addition, the intensity of this peak indicates that the graphite structure in the ACTF was acid-oxidized without significant damage, since any decrease in the order of crystallinity in ACTF will make the XRD peaks broader, and will shift the peak diffraction towards lower angles. There are other characteristic peaks of graphite at 2θ of about 29°, 35° and 60° with C(100), C(004) and C(110) diffractions of graphite, respectively.

In Fig. 6(b), The X-ray of chitosan displayed a type of semi-crystalline in the presence of two main peaks at 2θ=12°and 20°. The type of semi-crystalline of clear chitosan has approved the existence of two peaks, one was located at 2θ-12° and the other is at 20°which are indicating the great level of crystalline shape. The crystallinity in chitosan is simply formed because of the abundance(-OH & -NH_2)groups in its configuration, which could form power fulinter& intra-molecular hydrogen bonds.

XRD of ACTF/Composition (Fig. 6c), exhibited only a broad beak pattern indicating that the ACTF was becoming semi-crystalline during the composite formation with chitosan. However, the characteristic peaks of chitosan do appear, revealing that after immobilization of the ACTF, the XRD profile is not changed, suggesting that the crystalline structure of the support almost changed after ACTF composite formation. Also, we can find the peak of ACTF was observed at 2θ of 11.5°, which was assigned to the crystal plane (001). These results further indicate that the ATF/C composites prepared successfully.

HR-TEM

HR-TEM image of ACTF (Fig. 7) shows a transparent sheet with the presence of folded regions at the edges and in between that having activated carbon cavities that increase the surface area of the carbon nanostructures. These discrete diffraction spots can be listed to the face-centered cubic structure of ACTF, which unambiguously confirm the top layer is ACTF [28].

It can be clearly observed from Fig. 7 that, the dark spots assigned to the ACTF nanoparticles was distributed in the nanostructured of ACTF matrix. The ACTF nanoparticles have an average diameter of around 20–40 nm[29].

The SAED pattern in Fig. 7, exhibit a wrinkled edge of ACTF, in addition, the presence of two clear and weak rings, could be explained as a hexagonal structure of diamond carbon. Besides, many bright discrete diffraction spots also exist in the SAED patterns.

SEM

The surface morphology of chitosan & ACTF/C composite were studied via scanning electron microscopy and are illustrated in Fig. 8.

Chitosan bio-sorbent (Fig. 8 a) shows an irregular and rough surface, including micro-pores and small fractures, into which the oxyanions can penetrate and better access the internal functional adsorptive sites. Porosity enables the second phase adsorption according to the intra-particle diffusion theory, which is further discussed in kinetics modeling. The bio-sorbent particles have an irregular bead-like shape (granular) [30].

On the other hand, SEM of ACTF/C composite in Fig. 8(b), exhibit that the composite has no granular shapes and irregular sizes, i.e., the morphology appears as a smooth and rough surface. In SEM images, the composite observes the brighter regions that represented the ACTF species, confirming the presence of carbon graphene sheets of ACTF covered and overlapped with chitosan chains. Thus, micro-mechanic retention cannot be considered a key factor when explaining the adhesion between chitosan and ACTF [31]. Scanning electron microscopic images detected blasting agent particles impacted in the chitosan surface after composite preparation.

Thermogravimetric analysis (TGA)

HR-TEM image of ACTF in Figure 7 shows, a transparent sheet with folded regions at the edges, and between those that have activated carbon cavities, which increase the surface area of carbon nanostructures.

The TGA of ACTF/C composite has two major mass losses as the behavior of chitosan, but the second mass losses are shifted to 600°C due to the presence of ACTF which have high thermal

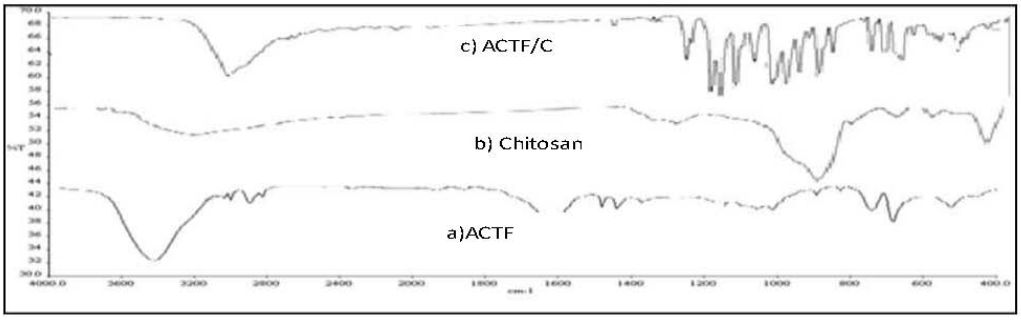

Fig. 5. FTIR of a) ACTF, b) Chitosan & c) ACTF/C composite.

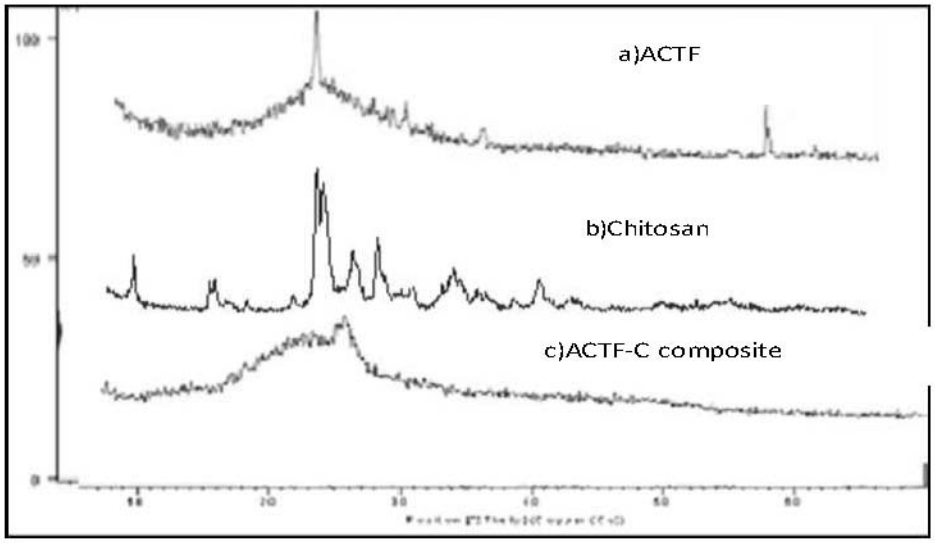

Fig. 6. XRD of a) ACTF, b) chitosan & c) ACTF-C composite.

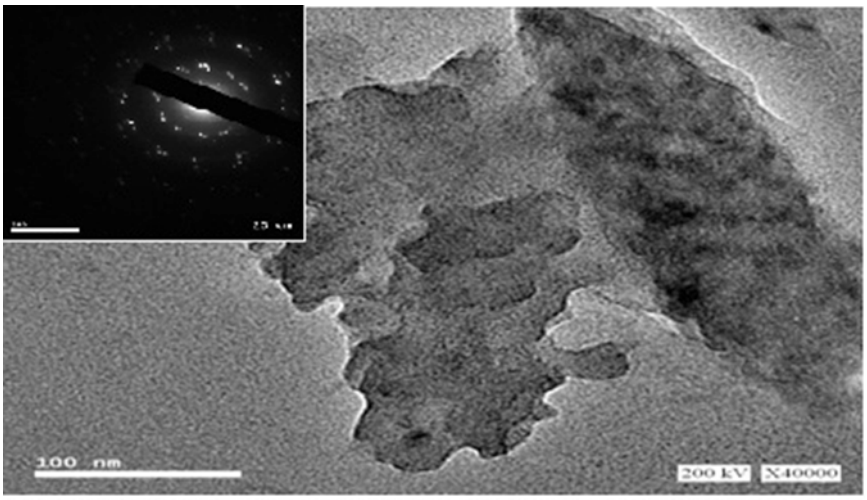

Fig. 7. HR-TEM of ACTF and SAED of ACTF/C composite.

stability. The results suggest that the prepared ACTF/C composite showed high thermal stability and that they could be utilized in the C–C coupling reactions.

Factors affecting the efficiency of the adsorption process. (Adsorption studies)

This study was conducted to improve the performance of ACTF/C in degrading organic pollutant, where methylene blue (MB) dye was used as a model of pollutant. The modification technique was done by applying reactive MB dye which acts as a sensitizer to the ACTF/C. Therefore, batch experiment was conducted to determine the suitability of prepared composite to remove MB from waste water, through dissolving 100 ml of MB dye into distilled water.

MB concentration was particularly selected as an optimal concentration that represented the maximum Nile contamination. To determine the effect of temperature on the dye removal from the experimental wastewater, four degrees of temperature were considered. Water sanitation in the middle region of the Nile Delta is far from ideality, as well as, the infections of the neglected dyes (such as MB), constitute a real risk factor for the populations. Overall, the discoveries of this work can be connected to treating industrial wastewater although further research should expand our concern of different aspects of the issue.

Effect of adsorbent dose

The dosage adsorbents ranged from 0.05 to 0.25 g / 100 ml (ppm). Figure 10 shows that MB removal efficacy significantly increased by increasing the adsorption dose from 0.05 /100 ml to 0.25 g / 100 ml. This may be owing to the accessibility of more adsorbed spots beside the accessibility of greater adsorption surfaces (Fig. 10). However, there were no substantial changes in the removal efficiency above the adsorption dose of 0.2 g/ 100 ml with removal efficacy value 78 Due to the adsorption conglomerate particle, thus, there is no growth in the effective surface area of the ACTF/C composite [33]. Consequently, 0.25 g/100 ml is supposed to be an optimum dose for the ACTF/C composite.

Effect of Different Initial Concentration

In this study, the effects of MB concentration on percentage removal were examined using initial MB concentrations of (10, 25, 50&100 ppm). From Fig. 11, it is observed that as the initial concentration of dye increases from 10 to 100 ppm, composite sorption capacity of ACTF/C increases, and the removal percentage increases from 9% (adsorption capacity ranging from 8 to 80 mg/g) to 80 % at 100 ppm. These sorption properties deduced that surface saturation is dependent on the initial dye concentration. As the dye concentration increments, adsorption capacity also increases because it provides a driving force to overcome the mass transfer resistances of dyes between the aqueous and solid phase. At a higher dye concentration, the dye ions are adsorbed more than at lower dye concentration, as more binding sites of the sorbent are free for interaction at low dye concentration and due to the rise in the mass transfer from the concentration gradient [34].

Effect of contact time

This effect did at (20-80 min) and shown in Fig. 12. The removal takes place during 70 minutes for the ACT/C composition, as shown in the figure, the removal of the dye was increased with increasing the time until it reaches the equilibrium at 40 min. Then it was slightly increased by 700 min. to reach 80%. The adsorption rate was primarily a consequence of the fact that all adsorbents are not taken and the concentration of the solution increased [28, 35]. Later on, the adsorption rate was reduced owing to an increase in the number of adsorbed spots and a decrease in dye concentration.

Effect of pH

The pH dye solution effect has a significant impact on MB adsorption on the ACTF/ Composite. As the hydronium (H_3O^+) and hydroxyl (OH^-) ions are effectively absorbed onto the surface of the adsorbent, the pH of the solution becomes effective in the adsorption of other ions.

The effect of pH on the adsorption of MB on ACTF/C composite adsorbent was tested at an initial pH value ranging from 2 to 9 and the results are plotted in Fig. 13.

At pH 9greatest removal of MB was detected. The aqueous solution of based will have a positive ionic charge in an acidic medium which tends to resist adsorption of MB dye. By increasing the pH medium the surface will get a negative charge, which results in increasing the adsorption of MB (due to the increased electrostatic attraction between the positively colored electrodes and the negatively charged adsorbent) [36].

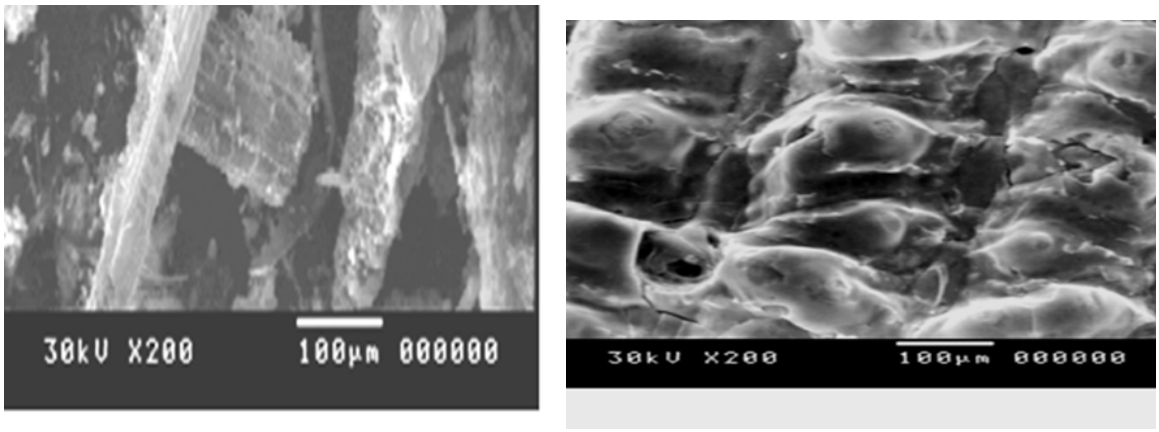

(a) (b)

Fig. 8. SEM of a) Chitosan & b) ACTF-C composite.

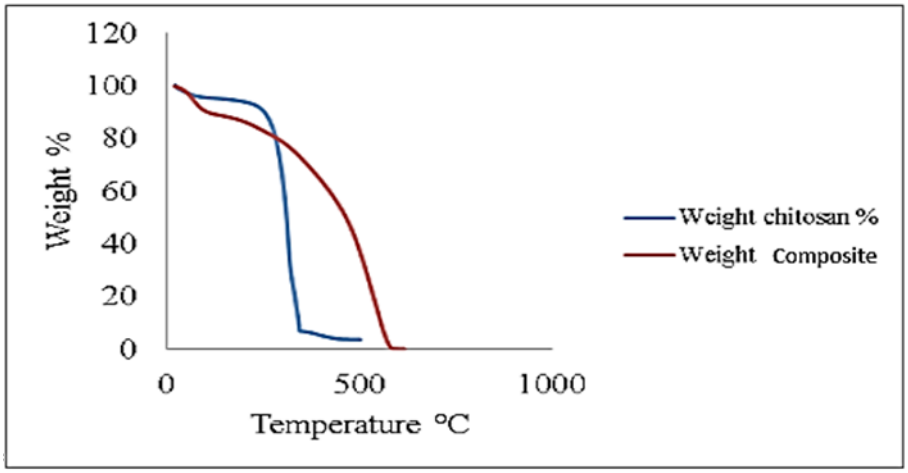

Fig. 9. TGA of chitosan and ACTF or composite.

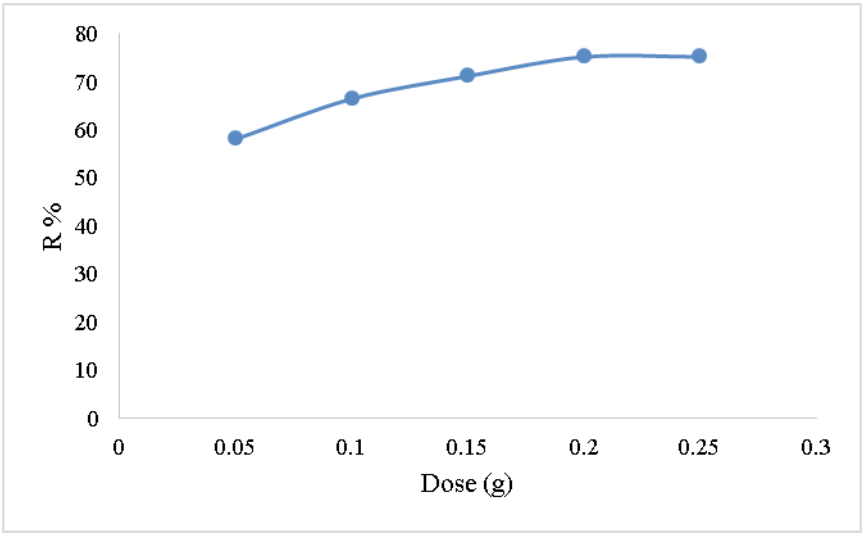

Fig. 10. The effect of adsorbent dose on the removal of MB dye.

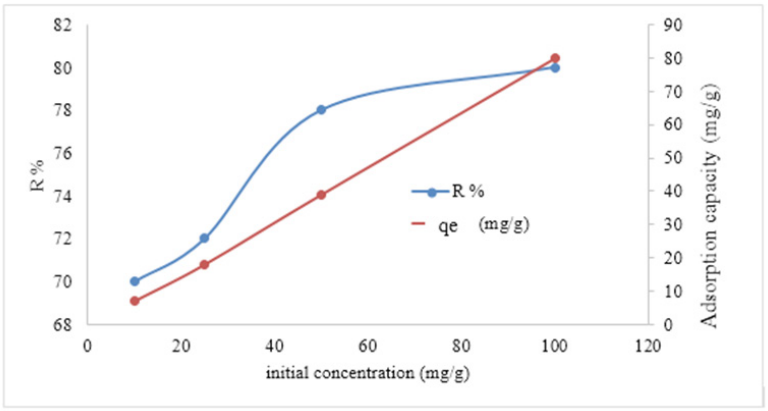

Fig. 11. Effect of different initial concentration on the adsorption capacity

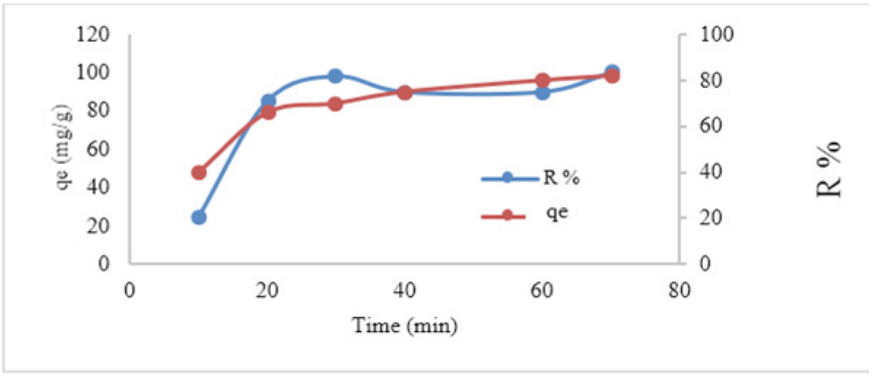

Fig. 12. Adsorption capacity and percent removal of dye at different contact time.

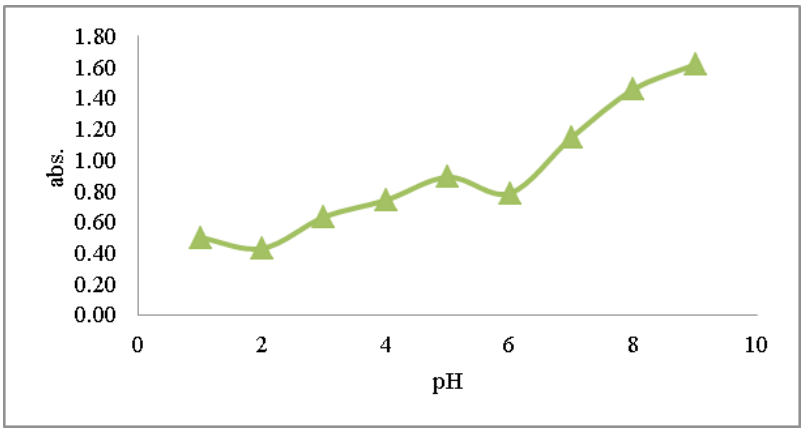

Fig. 13. The pH effect on MB adsorption.

Adsorption Kinetics

The pseudo-first order (Equation 6) and pseudo-second order (Equation 7) kinetic models were used to fit the experimental data.

$$\ln(q_e - q_t) = \ln q_e - K_1\, t \qquad (6)$$

where q_e is the adsorption capacity (mg/g) at equilibrium, qt is the adsorption capacity at time t, k_1 (1/min) is the pseudo-first-order adsorption rate constant, [31].

$$\frac{t}{q_t} = 1/(K_2 q_e^{\,2}) + t/q_e \qquad (7)$$

where q_e is the quantity of adsorbate adsorbed at equilibrium (mg/g), qt is the quantity of adsorbate adsorbed at contact time t (mg/g) and k_2 is rate constant of pseudo-second order (g/mgmin).

Kinetic studies were carried out by pulling and analyzing samples over a time interval every 5 minutes during the first 60 minutes, and then every 10 minutes until successive concentrations of the remaining dyes reach. Kinetic data for the adsorption of MB into a composite with four initial dye concentrations (10, 25, 50, and 100 mg/L) were tested with well-known kinetic models, namely pseudo-first order model and pseudo-second regular model. The mechanism of the adsorption process was studied by placing data with models. The parameters of these kinetic models are shown in Table 1 and Fig. 14.

The data on kinetic data based on pseudo-first and pseudo-secondary models are shown in Table 1. Based on high correlation coefficients, pseudo-second kinetic models can effectively describe MB absorption behavior of the composite. This illustrates that MB adsorption on the prepared composite is controlled by hemi-sorption processes. Based on the above results, we can assume that the MB adhesive mechanism on the composite can continue with the hemispheric processes that can pass through the formation of monolithic MB molecules on the surface of the composite.

Isothermal studies (Adsorption isotherm)

The equilibrium data in this experiment were analyzed by fitting it into two isotherm models at 25 C. The isotherm models used are the Langmuir and the Freundlich isotherm model. The difference between the quantity of material adsorbed at a constant temperature and the fastest solution is the connection to the isotherm system. Equilibrium isothermal equations balances are used to identify the sales data balance. Standards from different models give information on calculating and connecting dyes and design characteristics[37]. The Langmuir isotherm is mostly used in the field of relative thermodynamics relativity from physical aesthetics.

The adsorption capacity (q_m) was determined to be 48.62 mg/g (Table 2) (Eq. 3). Higher values of the correlation coefficient (0.996) indicate the applicability of the Langmuir isotherm, which means a uniform layer range and a uniform distribution of activity on the surface of the sorbent. In this study, values of R_L ($0 < R_L < 1$) favor MB adsorption for ACTF/C (see Table 2). This is useful for the adsorption of contaminants to adsorb one layer for a specific homogeneous region [38].

Equilibrium data are also set in the Freundlich equation (5). The parameters K_F and n indicate the adsorption capacity and the system adsorption strength. The size of the term (1/n) indicates the advantage of the adsorbent/adsorbate system. The correlation coefficient (0.871) is lower than the Langmuir value. Therefore, adsorption to ACTF/C does not follow the Freundlich isotherm [39].

The model shows the adsorption isotherms used for MB and the relevant parameters are shown in Table 2 and Fig. 15. If the R^2 value is less than 0.90, it indicates that it is not appropriate to describe the MB adsorption procedure for this point.

Thermodynamic studies

Thermodynamic parameters are the free energy ΔG^0, enthalpy change ΔH^0 &entropy change ΔS^0were calculated using the following using the relations:

$$\Delta G^0 = -2.303\ RT \log K_d \qquad (7)$$

$$K_d = q_e/C_e \qquad (8)$$

$$\Delta G^0 = \Delta H^0 - T\Delta S^0 \qquad (9)$$

$$\ln K_d = (\Delta S^0/R) - (\Delta H^0/RT) \qquad (10)$$

where q_e is a concentration of MB at equilibrium onto the composite (ppm), C_e is a concentration of MB at equilibrium in solution (ppm)& R is the universal gas constant (8.314

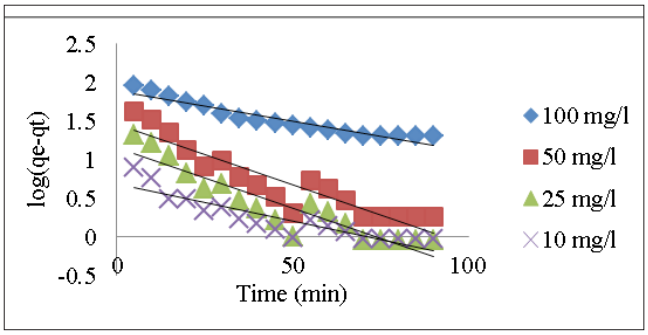

a)

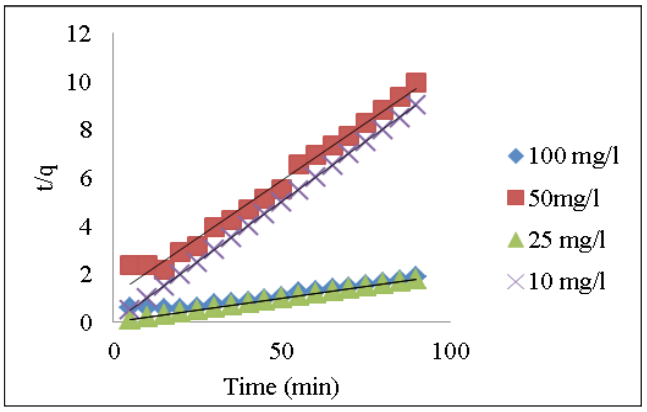

b)

Fig. 14. a) pseudo 1st order & b) 2nd order model for the adsorption of MB onto composite

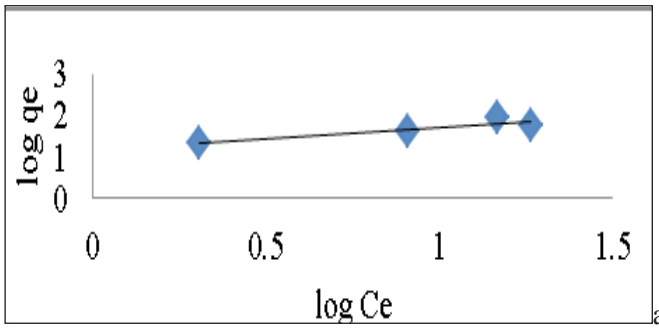

a)

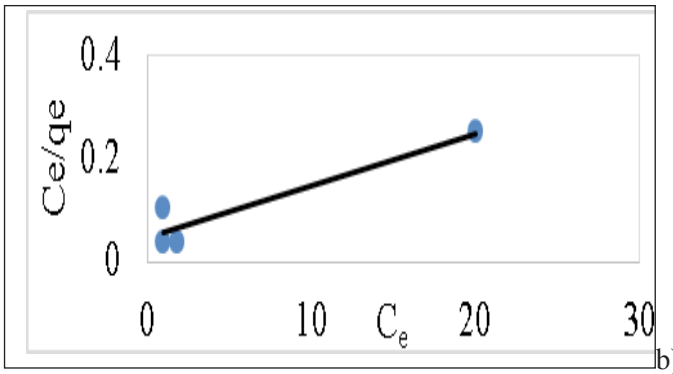

b)

Fig. 15. a) Freundlich & b) Langmuir isothermal model for the adsorption of MB onto composite.

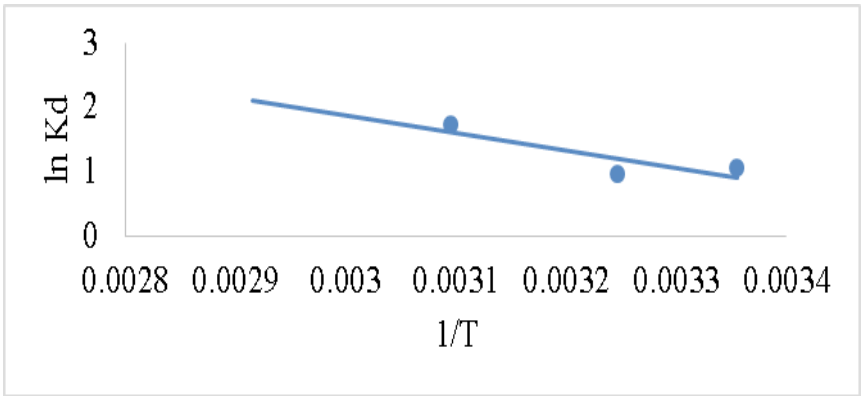

Fig. 16. Plot of lnKd vs. 1/T for the methylene blue adsorption on composite.

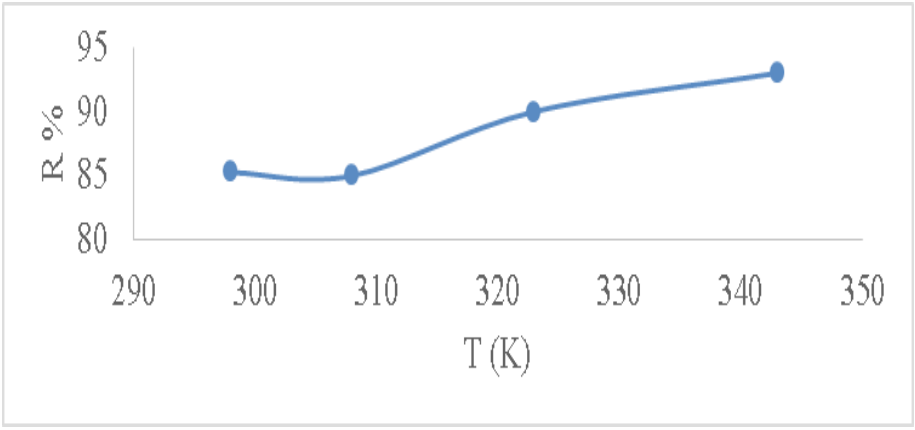

Fig. 17. Adsorption of M.B on composite at different temperatures.

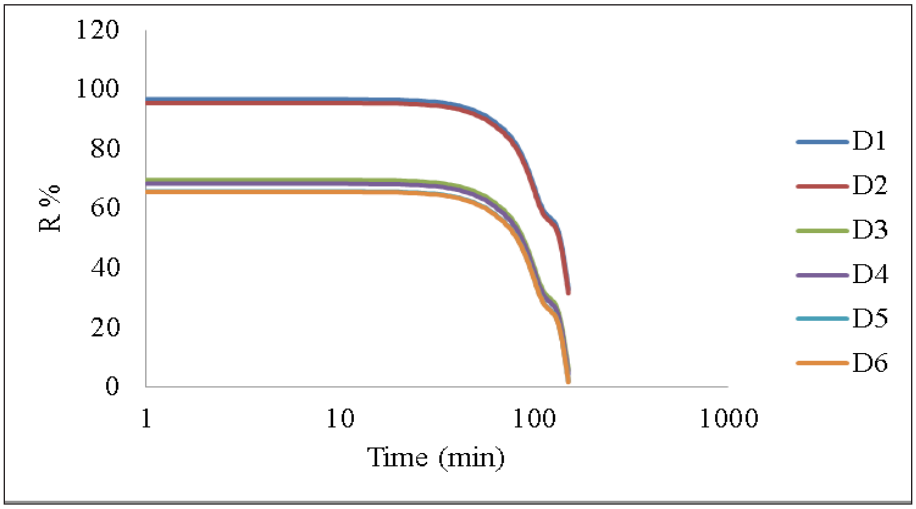

Fig. 18. Adsorption capacity for MB on composite for 6 adsorption–desorption cycles.

TABLE 1. Adsorption kinetic parameters for ACTF/C composite .

	C_0	K_1	q_e	R_2
pseudo 1st order	100	0.00791	0.277433	0.95615
	50	0.01575	0.166248	0.92754
	25	0.01575	0.066459	0.92754
	10	0.00951	0.16601	0.89914
	C_0	k_2	q_e	R_2
pseudo2nd order	100	0.016603	60.22883	0.981515
	50	0.095493	10.47201	0.99347
	25	0.02	50	1
	10	0.1	10	1

TABLE 2. The Isotherm constants of Langmuir and Freundlich isotherms for bio-sorption of methylene blue on composite.

Models	Isotherm constants		
Langmuir	q_m (mg g^{-1})	K_L (L mg^{-1})	R_2
	0.068052	0.014231	0.996201
Freundlich	k_F	n	R_2
	0.511083	1.20006	0.914358

TABLE 3. Thermodynamic parameters for the bio sorption of methylene blue on composite.

T	ΔS^0	ΔH^0	ΔG^0
298	164.8957	54260.8	-103399.758
308			-105048.715
318			-107522.151
328			-110820.065

J/mol K). The values of ΔH and ΔS were determined from the slope and intercept of the plot of $\ln K_d$ versus 1/T (Fig. 16). The adsorption of dye rises quickly with the rise in temperature from 298 to 328 K (Fig. 17). As shown in Fig. 17, adsorption of MB is all increased with increasing temperature, indicating that adsorption of this dye on the composite adsorbent was an endothermic process. This could be due to, the improved motion and dispersion of MB dye particles within the (ACTF/C) porous configuration get over the activation energy boundary, and/or an increase in dimerization of reactive dyes in solution values of the corresponding thermodynamic parameters, as shown in Table 3. It can be found that all values of ΔG^0 for MB are negative, which means that their adsorption processes are spontaneous[39, 40]. The values of ΔH^0 and ΔS^0 for MB are positive, implying that its adsorption on this composite is endothermic, and there is a decrease in randomness at the solid/liquid interface during the adsorption process.

Desorption and regeneration study

Simple recovery and long-term reuse of adsorbents is an important aspect of any practical industrial application because it reduces wastewater treatment costs and reduces the problem of waste disposal. In conventional practice, desorption experiments were carried out using desorption solvents, including acid. However, after recovering the desired material, the fate of desorption solvents carrying chemicals is unlikely. Therefore, in order to overcome the problem, in this research, a chemical-free method is adopted. Consequently, desorption experiments were performed with ultrasonic energy, as

mechanical vibrations cause the removal of the ionic color from the binding site[25].

Dye desorption is almost complete within 150 minutes as shown in Fig. 18, which is quick and Fast desorption indicates the physical nature of the adsorption process. The efficiency of dye desorption is calculated as 90.11% in the first cycle, and the second shows the re-use of ACTF nanoparticles. Re-use of the adsorbent was tested several times with absorption-desorption experiment. The results show that the adsorption capacity of the composite is subsequently reduced after each absorption and desorption cycle. Removal of % adsorbent on 6 cycles was more than 66% indicating that a similar adsorbent can be effectively used three consecutive times.

Conclusion

1) This article shows that ACTF/C composites can be used as low-cost adsorbent.

2) The maximum adsorption capacity of the composite is 85 mg/g at an initial concentration of 100 ppm

3) Contact time that maximum adsorption takes place within the first 70 min for ACTF/C composite.

4) Adsorption dosage is observed that 0.25 g/100 ml. Effect of pH shows that maximum adsorption happens in pH 9.

5) Adsorption of MB is all increased with increasing temperature, hence it is endothermic for ACTF/C composite adsorption.

6) Equilibrium isotherm study explains based on the Langmuir model that demonstrates the monolayer adsorption onto the composite.

7) The most suitable kinetic model for methylene blue adsorption is the pseudo-second-order model.

8) Thermodynamic study shows that Gibbs free is negative for ACTF/C composite it indicates adsorption is spontaneous and endothermic.

9) The composite is a promising adsorbent in the adsorption of methylene blue from aqueous solution and it will be applied in the future to real pollute water from some parts of the Delta governorates in Egypt.

References

1. Khanday, W., M. Asif, and B. Hameed, Cross-linked beads of activated oil palm ash zeolite/chitosan composite as a bio-adsorbent for the removal of methylene blue and acid blue 29 dyes. *International Journal of Biological Macromolecules,* **95**, 895-902 (2017).

2. El-Defrawy, M.M., et al., Adsorption of the anionic dye (Diamond Fast Brown KE) from textile wastewater onto chitosan/montmorillonite nanocomposites. *Egyptian Journal of Chemistry,* (2019)

3. He, X., et al., Removal of direct dyes from aqueous solution by oxidized starch cross-linked chitosan/silica hybrid membrane. *International Journal of Biological Macromolecules*, **82**, 174-181 (2016).

4. Chakravarty, P., K. Bauddh, and M. Kumar, Remediation of dyes from aquatic ecosystems by biosorption method using algae, in *Algae and Environmental Sustainability*, Springer. p. 97-106 (2015).

5. Malhat, F.M. and I. Nasr, Metals in water from the River Nile tributaries in Egypt. *Bulletin of Environmental Contamination and Toxicology,* **88**(4), 594-596 (2012).

6. Mahmoud, E.K. and A.M. Ghoneim, Effect of polluted water on soil and plant contamination by heavy metals in El-Mahla El-Kobra, Egypt. *Solid Earth,* **7**(2), 703-711 (2016).

7. Hosny, R., et al., Treatment of the oily produced water (OPW) using coagulant mixtures. *Egyptian Journal of Petroleum,* **25**(3), 391-396 (2016).

8. Ibrahim, A., G.F. El Fawal, and M.A. Akl, Methylene Blue and Crystal Violet Dyes Removal (As A Binary System) from Aqueous Solution Using Local Soil Clay: Kinetics Study and Equilibrium Isotherms. *Egyptian Journal of Chemistry,* **62**(3), 941-954 (2019).

9. Altundag, H., E. Bina, and E. Altıntıg, The levels of trace elements in honey and molasses samples that were determined by ICP-OES after microwave digestion method. *Biological Trace Element Research,* **170**(2), 508-514 (2016).

10. Metwally, B.S., et al., Fabrication, Characterization, and Dye Adsorption Capability of Recycled Modified Polyamide Nanofibers. *Egyptian Journal of Chemistry,* **61**(5), 867-882 (2018).

11. Wu, Z.-C., et al., A new porous magnetic chitosan modified by melamine for fast and efficient adsorption of Cu (II) ions. *International Journal of Biological Macromolecules,* **81**, 838-846 (2015).

12. Liu, X. and L. Zhang, Insight into the adsorption mechanisms of vanadium (V) on a high-efficiency biosorbent (Ti-doped chitosan bead). *International Journal of Biological Macromolecules*, **79**, 110-117 (2015).

13. Khan, S.B., et al., CuO embedded chitosan spheres as antibacterial adsorbent for dyes. *International Journal of Biological Macromolecules,* **88**, 113-119 (2016).

14. Wang, Z., et al., Kinetics of adsorption of bovine serum albumin on magnetic carboxymethyl chitosan nanoparticles. *International Journal of Biological Macromolecules,* **58**, 57-65 (2013).

15. Albadarin, A.B., et al., Activated lignin-chitosan extruded blends for efficient adsorption of methylene blue. *Chemical Engineering Journal,* **307**, 264-272 (2017).

16. Pathania, D., S. Sharma, and P. Singh, Removal of methylene blue by adsorption onto activated carbon developed from Ficus carica bast. *Arabian Journal of Chemistry*, **10**, S1445-S1451 (2017).

17. Altıntıg, E., et al., Effective removal of methylene blue from aqueous solutions using magnetic loaded activated carbon as novel adsorbent. *Chemical Engineering Research and Design,* . **122**, 151-163 (2017).

18. Altıntıg, E., et al., Production of activated carbon from rice husk to support Zn2+ ions. *Fresenius Environ. Bull.,* **24**(4), 1499-1506 (2015).

19. Fathy, M., T.A. Moghny, and M.A. Mousa, Fast and Fully Scalable Synthesis of Graphene Oxide from Cellulose by Catalytic Acid Spray Method (CAS). *Arabian Journal for Science and Engineering,* **44**(1), 305-313 (2019).

20. Fathy, M., et al., Synthesis of Transparent Amorphous Carbon Thin Films from Cellulose Powder in Rice Straw. *Arabian Journal for Science and Engineering,* **42**(1), 225-233 (2017).

21. Mahmoud Fathy, T.A.M., Mahmoud Ahmed Mousa, Abdel-Hameed A-A. El-Bellihi, Ahmed E. Awadallah, Synthesis of Transparent Amorphous Carbon Thin Films from Cellulose Powder in Rice Straw. *Arabian Journal for Science and Engineering* (2016) DOI: 10.1007/s13369-016-2273-5.

22. Huyen, N.T.M., et al. Synthesis of chitosan/graphene oxide nanocomposites for methylene blue adsorption. in *AIP Conference Proceedings*. AIP Publishing (2017).

23. Olajire, A.A., A.A. Giwa, and I.A. Bello, Competitive adsorption of dye species from aqueous solution onto melon husk in single and ternary dye systems. *International Journal of Environmental Science and Technology,* **12**(3), 939-950 (2015).

24. El Nemr, A., et al., Removal of direct blue-86 from aqueous solution by new activated carbon developed from orange peel. *Journal of Hazardous Materials,* **161**(1), 102-110 (2009).

25. Badruddoza, A., et al., Synthesis of carboxymethyl-β-cyclodextrin conjugated magnetic nano-adsorbent for removal of methylene blue. *Colloids and Surfaces A: Physicochemical and Engineering Aspects,* **367**(1-3), 85-95 (2010).

26. Dural, M.U., et al., Methylene blue adsorption on activated carbon prepared from Posidonia oceanica (L.) dead leaves: Kinetics and equilibrium studies. *Chemical Engineering Journal,* **168**(1), 77-85 (2011).

27. Luo, Y. and Q. Wang, Recent advances of chitosan and its derivatives for novel applications in food science. *Journal of Food Processing & Beverages,* **1**(1), 1-13 (2013).

28. Kumar, P.S., S. Ramalingam, and K. Sathishkumar, Removal of methylene blue dye from aqueous solution by activated carbon prepared from cashew nut shell as a new low-cost adsorbent. *Korean Journal of Chemical Engineering,* **28**(1), 149-155 (2011).

29. Theydan, S.K. and M.J. Ahmed, Adsorption of methylene blue onto biomass-based activated carbon by FeCl3 activation: Equilibrium, kinetics, and thermodynamic studies. *Journal of Analytical and Applied Pyrolysis,* **97**, 116-122 (2012).

30. Chen, D., et al., Removal of methylene blue and mechanism on magnetic γ-Fe2O3/SiO2 nanocomposite from aqueous solution. *Water Resources and Industry,* **15**, 1-13 (2016).

31. Saleh, T.A., M. Tuzen, and A. Sarı, Polyethylenimine modified activated carbon as novel magnetic adsorbent for the removal of uranium from aqueous solution. *Chemical Engineering Research and Design,* **117**, 218-227 (2017).

32. Shahabuddin, S., et al., Synthesis of chitosan grafted-polyaniline/Co 3 O 4 nanocube nanocomposites and their photocatalytic activity toward methylene blue dye degradation. *RSC Advances,* **5**(102), 83857-83867 (2015).

33. Senthilkumaar, S., et al., Adsorption of methylene blue onto jute fiber carbon: kinetics and equilibrium studies. *Journal of Colloid and Interface Science,* **284**(1), 78-82 (2005).

34. Amuda, O.S., et al., Adsorption of methylene blue from aqueous solution using steam-activated carbon produced from Lantana camara stem. *Journal of Environmental Protection*, **5**(13), 1352 (2014).

35. Marrakchi, F., et al., Mesoporous-activated carbon prepared from chitosan flakes via single-step sodium hydroxide activation for the adsorption of methylene blue. *International Journal of Biological Macromolecules,* **98**, 233-239 (2017).

36. Mahmoud, M.E., et al., Assessment of the adsorptive color removal of methylene blue dye from water by activated carbon sorbent-immobilized-sodium decyl sulfate surfactant. *Desalination and Water Treatment,* **57**(18), 8389-8405 (2016).

37. AL-Aoh, H.A., et al., Adsorption of methylene blue on activated carbon fiber prepared from coconut husk: isotherm, kinetics and thermodynamics studies. *Desalination and Water Treatment,* **52**(34-36), 6720-6732 (2014).

38. Kurniawan, A. and S. Ismadji, Potential utilization of Jatropha curcas L. press-cake residue as new precursor for activated carbon preparation: application in methylene blue removal from aqueous solution. *Journal of the Taiwan Institute of Chemical Engineers,* **42**(5), 826-836 (2011).

39. Bhattacharyya, K.G. and A. Sharma, Kinetics and thermodynamics of methylene blue adsorption on neem (*Azadirachta indica*) leaf powder. *Dyes and Pigments,* **65**(1), 51-59 (2005).

40. Atheba, P., P. Drogui, and A. Trokourey, Adsorption Kinetics and Thermodynamics Study of Butylparaben on Activated Carbon Coconut Based. *Journal of Encapsulation and Adsorption Sciences,* **8**(02), 39 (2018).